Experimental investigation of void coalescence in metallic sheets containing laser drilled holes

Arnaud Weck, David Wilkinson

May 13, 2008

A. Weck
McMaster University, Department of Materials Science and Engineering. 1280 Main Street West, Hamilton, ON, Canada. weckag@mcmaster.ca

D. Wilkinson
McMaster University, Department of Materials Science and Engineering. 1280 Main Street West, Hamilton, ON, Canada.

Abstract

Although important, ductility remains difficult to predict and there is a tremendous need for more precise modelling. Progress in this field is hampered by a lack of quantitative experimental results to assess the validity of these models due to the stochastic nature of ductile fracture. In this paper, tensile tests have been carried out in a scanning electron microscope on model materials made of thin metallic sheets containing laser drilled holes. Depending on the material and hole configuration, different failure modes and strains are observed. The results show the importance of void spacing and orientation, constraining effects, materials yield stress and work hardening rate, and the competition between ductile fracture and shear localization. Finally, it is shown that the Thomason model for void coalescence is not appropriate to predict fracture of the model material. However, the McClintock model for void growth, and the Brown and Embury and the McClintock models for void coalescence provide relatively good predictions.

1 Introduction

The ductile fracture process which consists of the nucleation, growth and coalescence of voids during plastic deformation has been extensively studied in the literature (see [1, 2, 3] for the void nucleation; [4, 5, 6, 7, 8, 9, 10, 11] for the void growth and [6, 12, 13, 14, 15, 16, 17, 18, 19, 20, 21, 22, 23, 24, 25] for the void coalescence). However, there is still no complete theory of ductile fracture that covers all three phases of the process. A critical issue is the lack of systematic experimental ways to observe the coalescence of voids. Therefore we have very few quantitative experimental results making it difficult to assess the validity of the models developed in the literature. The reason for this resides in the stochastic nature of fracture, making it difficult to capture the coalescence event. Furthermore, the number of voids intervening in the final failure is too high (thousands) for an analysis of coalescence between individual voids to be investigated. Attempts to fabricate model materials that would simplify the study of the ductile fracture process have already been made. For example, metal matrix composites made of an aluminum matrix reinforced by uniform-sized zirconia [26] or alumina [27] spheres have been tested. These samples contain a limited number of reinforcing particles, thus controlling the number of holes being nucleated. These model materials are useful to study damage nucleation events but are of limited value when one wants to study the coalescence event in detail, because the samples still fail in a stochastic manner. Magnusen at al. [28] developed model materials by drilling holes through metallic sheets. This

methodology has been used by other groups [29, 30] to study void growth and coalescence in a controlled manner. The drilled sheets in these studies have hole diameters between 0.8 and 1.2 mm. This approach greatly simplifies the microstructure because of the limited number of holes, their more or less controlled positioning and the removal of the nucleation problem. However, these model materials contain holes that are much larger than those found in real materials, where the void sizes are ranging from 0.001 to 0.05 mm ([7]). In this paper we describe a detailed study of void coalescence using a new model material made of a single metallic sheet containing holes of micron dimensions. These are fabricated using a laser drilling process as described in [31]. The experimental results are then compared to the McClintock model for void growth and to the Brown and Embury, Thomason and McClintock models for void coalescence.

Table 1: Chemical composition of the aluminum magnesium alloy 5052.

Si	Fe	Cu	Mn	Mg	Cr	Zn	Ti	Other	Al
0.25	0.40	0.10	0.10	2.5	0.15	0.10	0.05	0.015	Rest

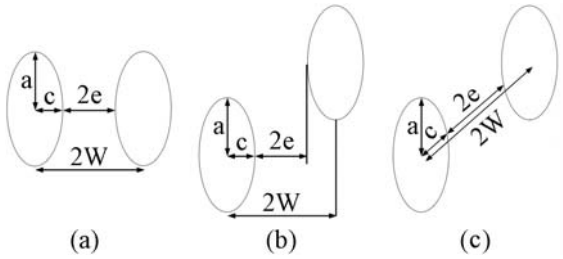

Figure 1: Schematic drawing showing how the various void dimension parameters are extracted depending on the hole orientation with respect to the tensile axis (vertical on the picture) (a) for holes normal to the tensile axis, (b) for holes at an arbitrary angle and (c) along the shearing direction.

2 Experimental methods

The material used is an Al-Mg alloy (AA5052) whose composition is shown in Table 1. The tensile sample has a dog-bone shape with a gage length of 4 mm, a width of 2 mm and a thickness of 0.1 mm. In the center of the sample, various laser drilled hole configurations were produced for which the laser holes run through the tensile sample and have a diameter of 10 μm. Having at least 0.5 mm of hole-free material on each side of the array enables better control on the sample failure. The samples were then polished using a 1 μm diamond paste and annealed at 345°C for 30 min to remove the effect of the heat affected zone around the holes (see [31] for a detailed presentation of this phenomenon). After annealing, the grain size is about 10 μm. Another material named Glidcop was also tested to investigate the effect of different properties on coalescence. This material consists of a copper matrix containing 0.25% by wt. of aluminum in the form of a fine dispersion (∼50 nm in diameter) of aluminum oxide particles. After laser drilling, the Glidcop samples are annealed at 1000°C for 30 minutes which resulted in a final grain size of about 10 μm. All tensile tests were carried out at a constant crosshead speed of 30 μm/s with the samples being pulled in-situ in a scanning electron microscope (SEM) which allowed pictures to be taken during the test. Both load and displacement were also recorded during the test. From the SEM images, quantitative information is extracted such as the hole spacing, the major and minor diameters of the holes and the ligament length as a function of the macroscopic strain. After the test, samples were mounted for SEM observations of the fracture surfaces.

3 Experimental results

3.1 Effect of the hole orientation

In order to study the influence of the initial hole geometry on hole growth and coalescence, in a simplified fashion, two holes have been drilled in the middle of aluminum tensile samples at respectively 90° and 45° with respect to the tensile direction. In these experiments, the holes spacing 2W (see Figure 1(a) and (b)) is respectively 37 μm and 26 μm so that the absolute distance between the center of the holes is the

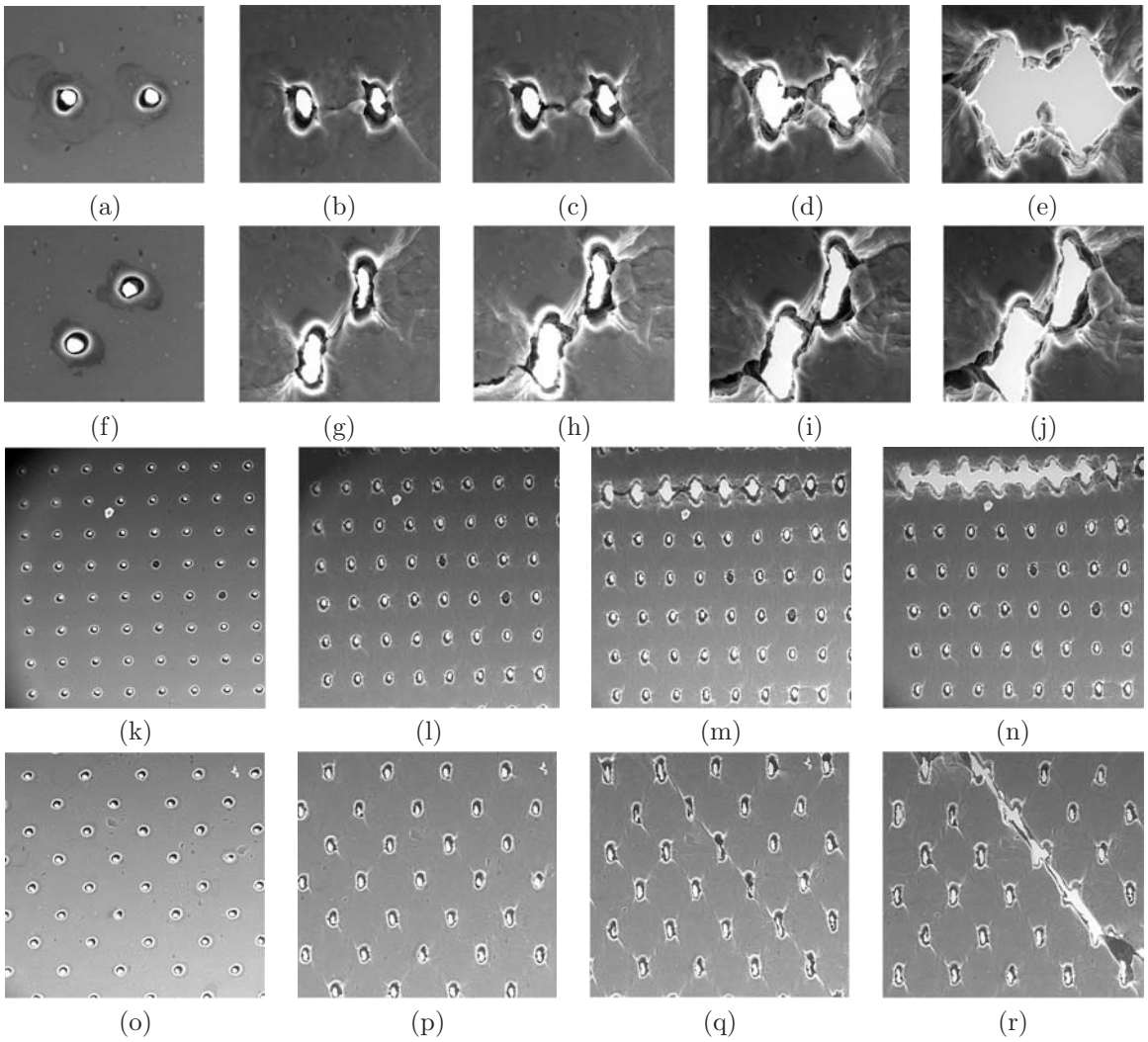

Figure 3: In-situ SEM images of the deformation sequence of aluminum alloy 5052 containing various hole configurations and taken at various far field true strains. Two holes oriented at 90° with respect to the tensile direction (vertical): (a) 0, (b) 0.204, (c) 0.213, (d) 0.220, (e) 0.223. Two holes oriented at 45° with respect to the tensile direction (vertical): (f) 0, (g) 0.233, (h) 0.234, (i) 0.235, (j) 0.237. Array of holes oriented at 90° with respect to the tensile direction (vertical): (k) 0, (l) 0.178, (m) 0.202, (n) 0.203. Array of holes oriented at 45° with respect to the tensile direction (vertical) (o) 0, (p) 0.176, (q) 0.216, (r) 0.221.

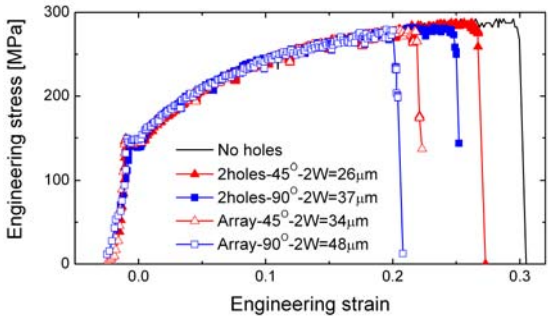

Figure 2: Engineering stress-strain curves for the 5052 aluminum alloy containing various hole configurations.

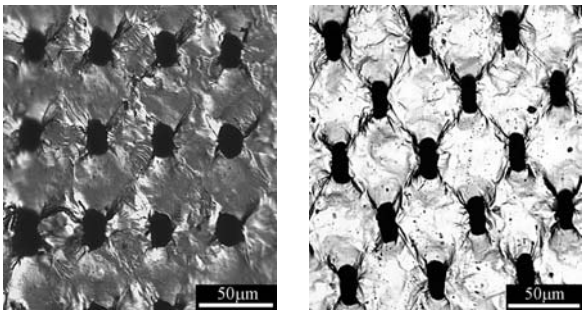

(a) (b)

Figure 4: Optical images in Normaski contrast showing the thickness deformation patterns in an array of holes oriented at (a) 90°, (b) 45° with respect to the vertical tensile axis.

same (37 μm) in each case. The engineering stress-strain curves for the two samples tested are plotted in Figure 2 and the engineering failure strains are shown in Table 2. As expected, the samples containing holes have a lower failure strain than the one without holes. One can also see that the sample with the holes oriented at 45° have more ductility compared to those with the holes aligned at 90°. Because of the low volume fraction of voids (∼1%), the macroscopic behavior of the samples is the same up to the coalescence of the voids. Some of the SEM images acquired during the tensile tests are shown in Figures 3(a-j). When the two holes are oriented at 90° with respect to the tensile axis, coalescence occurs by internal necking of the ligament between the holes. However, when the holes make a 45° angle with the tensile direction, coalescence proceeds through a shearing process. In order to verify that the same failure mechanisms are observed in arrays of holes, 13 by 13 hole arrays have been drilled with the same two orientations (90° and 45° with respect to the tensile axis). The results presented in Figures 3(n-r) show again that failure occurs by internal necking when the holes are at 90° and by shear when they are at 45°. The surface of the arrays at 90° and 45° has been observed under an optical microscope using Nomarksi contrast to better reveal the slip steps on the surface. These are shown in Figure 4 where the tensile direction is vertical. The contrast on the pictures shows the variations in depth resulting from the thinning of the samples in their thickness. It can be seen that plasticity is spreading between the holes for the sample with the array at 90° but is strongly localized between holes at 45° for the sample with the array at 45°. Looking at these slip lines tells us about the stress state in the sample. Indeed, if the stress state between the voids were plane strain, there would be no deformation of the samples in the thickness direction and thus no features would be visible on the sample surface.

The fracture surfaces of both arrays at 90° and 45° have been observed by SEM (Figure 5). One can see that the ligament between the voids has necked down to a line for the array at 90° with few secondary voids nucleated between the main laser holes. For the array at 45° the shearing process is clearly seen in Figure 5(c) in the lower part of the ligament. However the shearing did not occur over the whole length of the ligament because secondary voids are nucleated on the upper part of the ligament in Figure 5(c) suggesting that a normal type of failure occurred after about half of the ligament was sheared. The schematic drawing in Figure 6(a) details the steps leading to the fracture surface morphology seen in Figure 5(c). Experimental support for this failure mechanism is shown in Figure 6(b) which represents a close up from an array of holes oriented at 45°. There are two main explanations for the normal type of failure observed at the end of the ligament. The

first is that the constraining effect of the hole-free material (0.5 mm on either side of the array) prevents the material from completely shearing off at 45°. In addition, the shearing process creates a crack which induces a high stress triaxiality ahead of it. This high stress triaxiality is favorable for secondary void nucleation and growth leading to the dimpled fracture surface seen in Figure 5(c).

3.2 Effect of the hole spacing

Samples containing two holes at 90° to the tensile axis and spaced 15, 25, 40 and 50 μm from each other have been tested in situ to study the effect of the hole spacing on coalescence. The engineering failure strains are shown in Table 2 for the various hole spacings $2W$ (last four lines of Table 2). The results are consistent and show that the closer the holes, the earlier the coalescence and the lower the final failure strain of the whole sample. The in-situ SEM images are shown in Figure 7. Only the pictures at the coalescence event (or final failure of the ligament between the holes) are shown. One can see that the larger the distance between the holes, the more the holes have to grow before coalescence can take place. Also, the further apart the holes, the more slip features are present on the sample surface, suggesting that the material had to deform more before the final coalescence. This is also related to the state of hardening of the material at the coalescence event. The more the sample has to be deformed prior to coalescence, the lower the work hardening rate gets, which favors coalescence. The features on the surface also tell us that the ligament between the holes might be in a state of plane strain when the holes are close to each other (Figure 7(a) and (b)) and that the stress state tends toward that of plane stress when the holes are further apart (Figure 7(c) and (d)). Indeed, Thomason [32] proposed that a plane strain condition between the voids is achieved when the through-thickness dimension h is at least five times the hole spacing $2e$ (h>10e). The sample thickness h is here always 100 μm and when the holes spacing 2W is 15 and 25 μm (Figure 7(a) and (b)), $2e$ is respectively 5 and 15 μm which correspond to the plane strain case (h>10e). However, for the larger hole spacings (2W=40 and 50 μm), h<10e

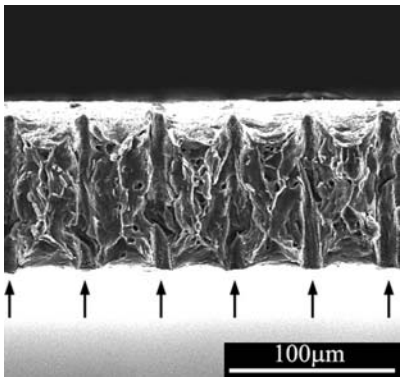

(a)

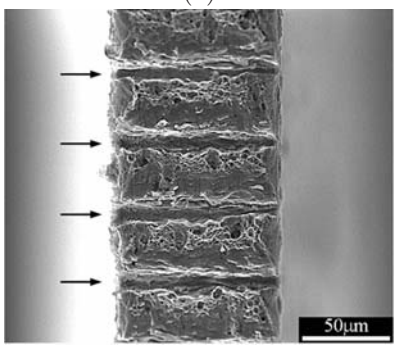

(b)

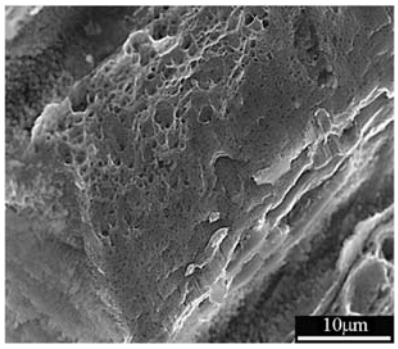

(c)

Figure 5: SEM images of the fracture surfaces of the samples tested in the SEM and containing arrays of laser holes oriented at (a) 90° and (b) 45° with respect to the tensile axis. The electron beam was perpendicular to the fracture surfaces in (a) and (b) when the images were acquired. A close up on the ligament between two holes from an array at 45° is shown in (c). The black arrows indicate the location of the laser holes.

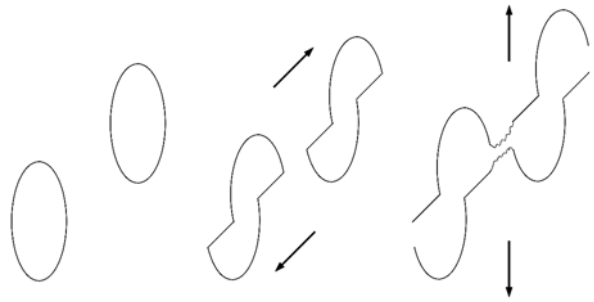

(a)

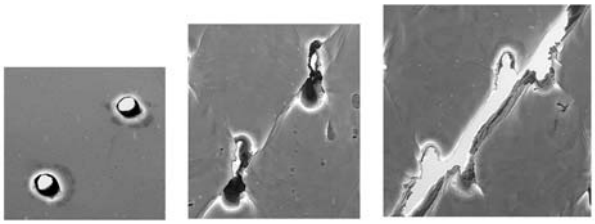

(b)

Figure 6: (a) Schematic drawing explaining the failure process of holes oriented at 45° with respect to the tensile axis (vertical). The shearing at 45° is followed by a normal type of failure due to constraining effects and the high stress triaxiality ahead of the crack. The arrows indicate the direction of local material flow. (b) Close-up on two holes from an array of holes oriented at 45° to the tensile axis (vertical).

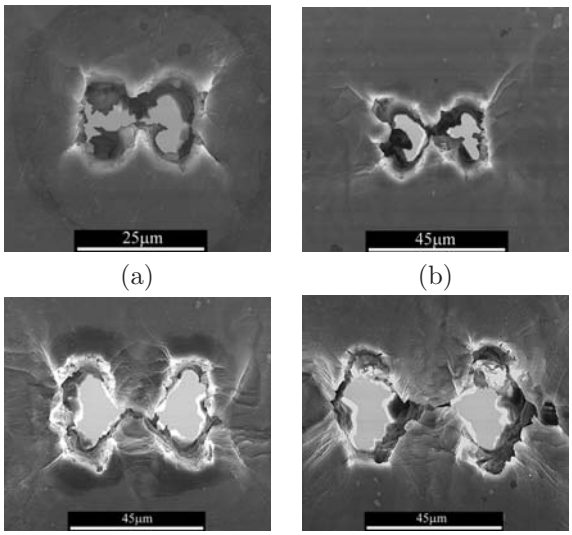

(a) (b) (c) (d)

Figure 7: SEM images of two laser holes at coalescence in 5052 aluminum alloy for initial hole spacings of (a) 15 μm, (b) 25 μm, (c) 40 μm and (d) 50 μm.

and the stress state in the ligament tends towards plane stress.

3.3 Effect of the number of holes

In order to check whether the number of holes affects the local strains at coalescence, samples containing 1, 3, 7 and 13 lines each with 13 holes perpendicular to the tensile direction and 40 μm apart have been tested. The engineering failure strains are shown in Table 2 and are in agreement with the results of Mulholland at al. [33] in that the macroscopic ductility of the the sample increases with the number of lines of holes. However, this does not mean that the local coalescence strain is affected by the other lines with holes. The higher overall ductility is simply an outcome of the geometry. Thus, the more lines with holes, the softer the material gets and the higher the contribution to the overall deformation. The contrary is observed when adding holes in the direction normal to the tensile direction. Indeed, if one compares the engineering failure strain of 2 holes at 90° to the tensile axis and 40 μm apart ("2holes-90°-2W=40 μm"

Table 2: Experimental engineering failure strains for various hole configurations.

Configuration	Engineering failure strain
No holes	0.303
2holes-90°-2W=37 μm	0.251
2holes-45°-2W=26 μm	0.268
Array-90°-2W=48 μm	0.204
Array-45°-2W=34 μm	0.222
1 line-90°-2W=40 μm	0.174
3 line-90°-2W=40 μm	0.182
7 line-90°-2W=40 μm	0.195
13 line-90°-2W=40 μm	0.209
2holes-90°-2W=15 μm	0.224
2holes-90°-2W=25 μm	0.233
2holes-90°-2W=40 μm	0.242
2holes-90°-2W=50 μm	0.255

in Table 2) to the failure strain of a line with 13 holes also spaced 40 μm apart ("1line-90°-2W=40 μm" in Table 2), one can see that there is a 30% decrease in the macroscopic failure strain when going from 2 holes to 13 holes in a line. But again, whether these differences are true locally will be investigated in section 4.

3.4 Effect of the material properties

An SEM image of the Glidcop sample after failure is shown in Figure 8. One can see that the ligament between the holes does not neck down to a line as in the case of the aluminum samples. Also, the length of the holes at coalescence is 2a=28 μm for a distance between the holes centers of 2W=40 μm. This value is much lower than that found for the aluminum sample where 2a=36 μm. Furthermore, coalescence does not occur between the holes but rather localization takes place in the thickness direction as shown in Figure 8 even though the distance between the holes (40 μm) is smaller than the sample thickness (100 μm). The reasons for these differences between coalescence strains and failure paths are twofold. First the fine dispersion of alumina particles in the Glidcop sample nucleates a second population of voids that ultimately precipitates coalescence between the main laser drilled holes. For the second explanation, we assume localization in terms of the localized necking proposed by Hill [34] and defined as $d\sigma/d\varepsilon=\sigma/2$. The work hardening rates of the aluminum and Glidcop samples are not too different but the main difference is their yield stress which for the Glidcop samples is $\sigma_Y \approx 500$ MPa and for the aluminum sample $\sigma_Y \approx 150$ MPa. Therefore, from the Hill analysis, localization will take place at a lower strain in the sample with higher yield stress, i.e. the Glidcop sample. Whether the secondary voids or the localization are responsible for the lower coalescence strains found in Glidcop is difficult to determine from these results. In the case of aluminum, because of its low yield stress, and because almost no secondary voids are nucleated, the holes have time to grow to the required length for them to coalesce before localization can take place. However, for the Glidcop samples, because of its high yield stress and because secondary voids can be nucleated, the holes have not grown sufficiently to be able to coalesce and failure occurs by localization in the thickness direction. Therefore, there is a competition between ductile fracture and shear localization. Ductile fracture will be favored by low yield stress, high work hardening rate, low void nucleation strains and high void volume fraction.

4 Analysis of void geometry

From the SEM pictures taken in-situ during the tensile test, several parameters can be measured such as the major diameter of the void or void length $2a$, the ligament length $2e$ and the intervoid spacing or center to center separation of the voids $2W$ (see Figure 1). For better accuracy and consistency, the minor diameter of the voids $2c$ has not been measured but is calculated using $c = W - e$. It should be noted that the parameters a, e, W and c correspond to the current void dimensions and a_0, e_0, W_0 and c_0 to the initial void dimensions. The error in the measurements of these parameters from the SEM images is approximately 1 μm.

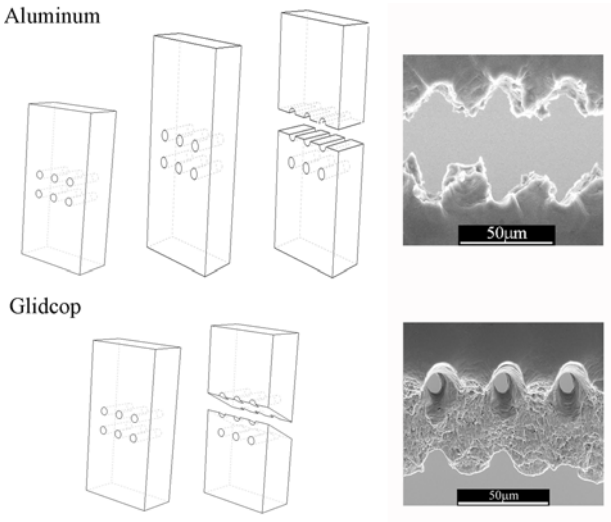

Figure 8: Schematic diagram showing the failure mechanisms in both aluminum and Glidcop samples and comparison with the experimental results. The aluminum sample fails by ductile fracture between the voids and the Glidcop sample by localization in the thickness direction.

4.1 Major diameter

Figure 9(a) shows the true local strain defined as $ln(a/a_0)$ as a functions of the true far field strain defined as $ln(1+e_{ff})$ where e_{ff} is the far field engineering strain. One can see that the closer the holes are from each other (smaller values of 2W), the earlier void growth accelerates and the smaller is the local true strain. This behavior is confirmed in Figure 9(b) where the local true strain at void growth acceleration is the same independently of the number of lines with holes in the tensile direction (as indicated by the horizontal dotted line). Therefore, even though the far field strains are different when void growth accelerates, because the distance between the holes is the same in all four configurations, the local true strains at the acceleration point are the same. If now the coalescence strain for 2 holes oriented at 90° ("2holes-90°-2W=40 μm" in Table 3) is compared to that for 13 holes ("1line-90°-2W=40 μm" in Table 3), one finds in both cases the same value of 1.25. These results confirm that for holes at 90° as long as the distance between holes is the same, the local coalescence strains will be the same, independent of the number of holes in the array. The results from Table 3 show another interesting result. For the case of 2 holes at 90° and with a hole spacing of 2W=40 μm, the local coalescence strain is lower than for the array of holes (2W=48 μm) mainly because in the array, the distance between the holes is larger. However, when the case of 2 holes at 45° and spaced by 2W=26 μm is compared to the array at 45° (2W=34 μm), one can see that now the coalescence strain is lower for the array even though the distance between the holes is larger. This is due to constraining effects of the hole-free material on each side of the array of holes that prevents the holes from shearing freely at 45°. Thus, the more holes are present at 45°, the less is the constraint and the more easily the sample can shear, hence the lower coalescence strains.

4.2 Ligament length

The normalized ligament length defined as e/e_0 is plotted against the true far field strain in Figures 10(a) and 10(b). We see that the ligament length

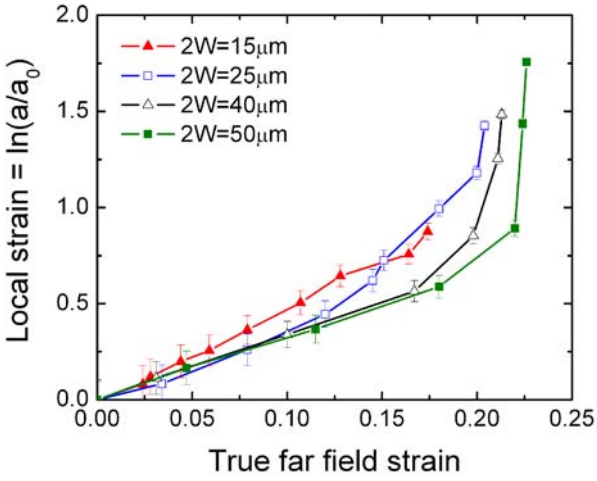

(a)

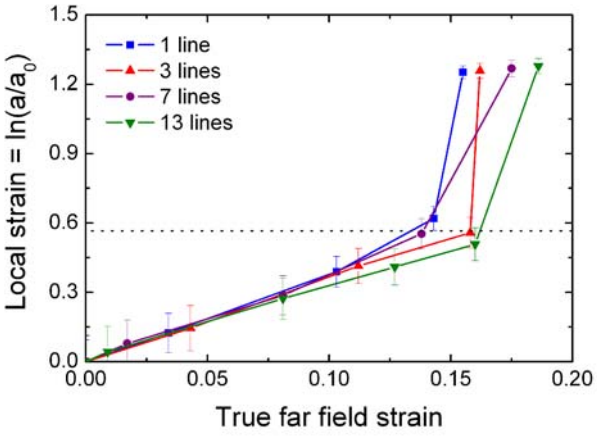

(b)

Figure 9: Local strain on the scale of the voids versus the true far field strain for holes drilled in a 5052 aluminum alloy and having (a) two holes at 90° to the tensile direction for various spacings 2W and (b) various number of lines in the tensile direction each of them containing 13 holes at 90° to the tensile direction and spaced 40 μm apart.

rapidly decreases at an earlier strain when the holes are closer together (Figures 10(a)). One can also conclude from Figures 10(b) that the important parameter is again the distance between the holes because when the distance is the same, the behavior of the ligament is the same.

4.3 Minor diameter

The normalized minor diameter defined as c/c_0 is plotted against the true far field strain in Figures 11(a) and 11(b). One can see that the minor diameter first decreases at low strains and then increases again due to the interaction between the voids that forces the voids to grow toward each other. When the distance between the holes is small enough, the holes start interacting almost from the beginning of the deformation and there is no minimum in the normalized minor diameter plots (Figure 11(a) when 2W=15). The further apart are the holes, the longer it takes for them to interact. Therefore, the minimum diameter in Figure 11(a) becomes smaller and moves to higher strain as the ligament spacing increases. Because the distance between the voids is the same in Figure 11(b), the behavior of the minimum diameter is the same.

4.4 Definition of coalescence

From the results presented in the previous sections, it is difficult to define coalescence as a function of geometrical parameters as these parameters vary smoothly with strain. The only curve that does show a well defined transition is that for the minor diameter (Figures 11(a) and (b)). When this parameter reaches its minimum value, this could be taken as the coalescence strain since it is the strain at which the holes start growing towards each other. However, these strains are rather small compared to what is generally thought of a coalescence strain. Physically, this suggests that the holes start to interact and grow toward each other before a strong localization (or coalescence) occurs. Furthermore, the minimum is very shallow making it difficult to determine with any accuracy. Therefore, we have not used a criterion based on the minimum value of the minor diameter of the

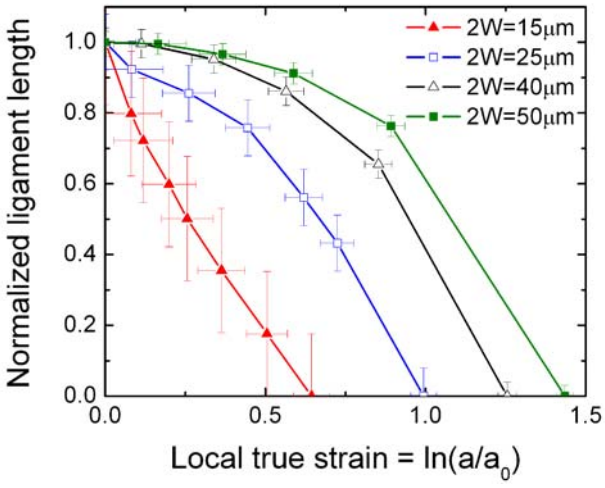

(a)

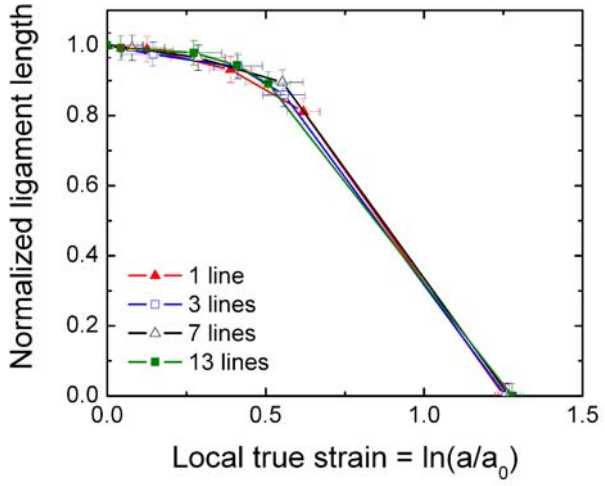

(b)

Figure 10: Normalized length of the ligament between the holes versus the true far field strain for holes drilled in a 5052 aluminum alloy and (a) two holes at 90° to the tensile direction for various spacings 2W and (b) various number of lines in the tensile direction each of them containing 13 holes at 90° to the tensile direction and spaced 40 μm apart.

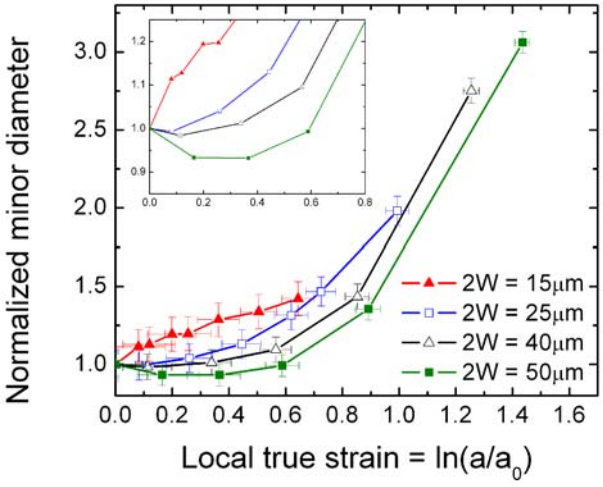

(a)

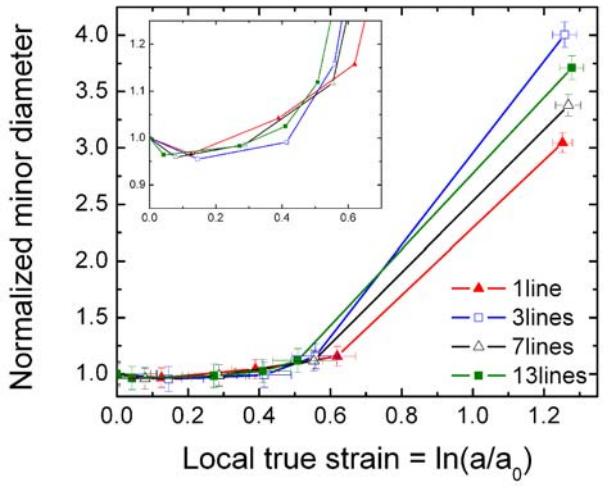

(b)

Figure 11: Normalized minor diameter of the holes versus the true far field strain for holes drilled in a 5052 aluminum alloy and having (a) two holes at 90° to the tensile direction for various spacings 2W and (b) various number of lines in the tensile direction each of them containing 13 holes at 90° to the tensile direction and spaced 40 μm apart. The inset in the figure is a close-up showing the decrease in minor diameter at small strains.

voids in further work. The only other criterion that is tractable in a precise way is the point of ligament failure. The assumption behind this criterion for coalescence (defined as a strong localization between the voids) is that the strain differences between the coalescence event and the fracture of the ligament are negligible. This is the criterion retained for the following section which compares the experimental coalescence strains to that of models in the literature.

5 Comparison with models in the literature

5.1 Void growth: McClintock Model

The void growth model for cylindrical voids proposed by McClintock [7] has been used in this study and is given by:

$$ln\left(\frac{R}{R_0}\right) = \frac{\bar{\varepsilon}\sqrt{3}}{2(1-n)}\sinh\left(\frac{\sqrt{3}(1-n)}{2}\frac{\sigma_1+\sigma_2}{Y}\right)+\frac{\varepsilon_1+\varepsilon_2}{2}$$

where R is the mean radius of the elliptical void, R_0 is the initial void radius, $\bar{\varepsilon}$ is the far field true strain. The applied stresses σ_1 and σ_2 are those in the principal directions and ε_1 and ε_2 are the corresponding strains. The strain hardening exponent n has been determined from the experimental stress-strain curve and is equal to 0.3.

For plane strain, $\varepsilon_2 = -\varepsilon_1$, $\sigma_1 = 2Y/\sqrt{3}$ and $\sigma_2 = Y/\sqrt{3}$. This reduces equation 1 to:

$$ln\left(\frac{R}{R_0}\right) = \frac{\bar{\varepsilon}\sqrt{3}}{2(1-n)}\sinh\left(\frac{3(1-n)}{2}\right) \qquad (1)$$

Comparison between equation 1 and the experimental results is presented in Figure 12. One can see that the McClintock model predicts rather well void growth at low applied far field strains. The prediction deteriorates at high strains because in the experiment, the voids start interacting and coalescing which accelerate void growth.

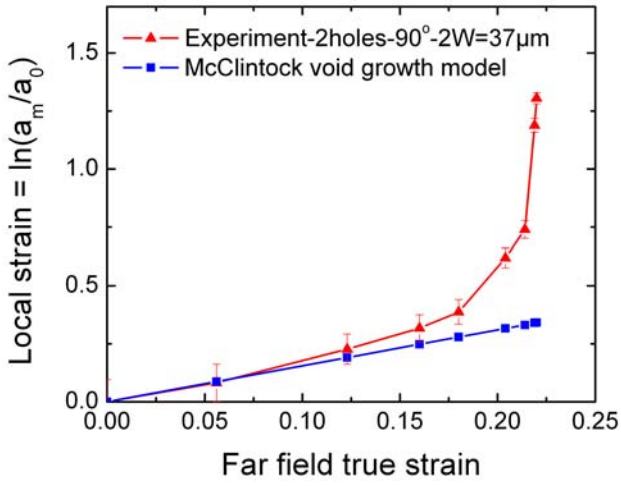

Figure 12: Comparison between the McClintock model predictions for void growth and the experimental results.

5.2 Void coalescence: Brown and Embury model

The Brown and Embury model [16] for ductile fracture states that coalescence occurs when shear bands at 45° can be drawn between the growing voids. This corresponds geometrically to the point at which the void length $2a$ is equal to the intervoid spacing $2W$. This model can be easily verified by plotting both the intervoid spacing and the void major diameter as a function of the local true strain. The intersection of these two curves will then provide the coalescence strain. The results are shown in Table 3. The Brown and Embury model is in excellent agreement with the experimental results except for the configuration at 45° and when the holes are close to each other. In the former case, a definition depending on hole orientation for the geometrical parameter $2W$ might be required. Using the hole geometry definitions shown in Figure 1(c) gives coalescence strain predictions of 1.15 and 1.46 for two holes at 45° and the array of holes at 45° respectively. These values are closer to the experimental ones with percentage differences of -15% and +10%. The remaining discrepancies are probably due to the geometrical constraint for holes

at 45° and discussed in section 3.1. Also, from the results in Table 3, we can see that there are larger variations between model and experiments when the distance between the voids is smaller; 2W=15 μm and 2W=25 μm. This is due to the fact that when the holes are closer to each other, they coalesce at lower strains and thus the work hardening is still important. The Brown and Embury model does not take into account the state of hardening of the material at coalescence, hence the discrepancy.

5.3 Normal void coalescence: Thomason model

The experimental hole configuration used here corresponds to the 2D version of the Thomason model ([32]) which states that the onset of microvoid coalescence takes place when the following equation is verified:

$$\left(\frac{0.3A_{n-2D}}{a/c(1-A_{n-2D})}+0.6\right)(1-V_f)^{-1}=\frac{\sigma_m}{Y}+\frac{1}{2} \quad (2)$$

where A_{n-2D} is the area fraction of intervoid matrix defined as $A_{n-2D}=e/W$, V_f is the initial void volume fraction defined as $V_f=(\pi/4)(c_0/W_0)^2$, σ_m is the mean stress and Y the plastic equivalent stress. The stress triaxiality σ_m/Y for the plane strain model is taken to be a constant equal to 1/2. To obtain the coalescence strain, the left hand side (LHS) and right hand side (RHS) of equation 2 are plotted against the local true strain and the intersection of these curves gives the coalescence strain. The results are shown in Table 3. The predictions of coalescence using the Thomason model are in average 45% lower than the experimental values. Some of the reasons for these large discrepancies are the plane strain assumption and the state of hardening of the material which is not taken into account. However, the main reason comes probably from differences in the definition of coalescence in the model and experimentally. This point will be further discussed in section 6.

5.4 Coalescence by shear: McClintock model

McClintock et al. [35] proposed a plane strain condition for coalescence in a localized shear band where the void linkage in the shearing direction occurs when:

$$\frac{2W}{2c}=exp\left[\frac{\sqrt{3}\bar{\varepsilon}}{2(1-n)}\sinh\frac{3(1-n)}{2}+\ln\sqrt{1+3\bar{\varepsilon}^2}\right] \quad (3)$$

where the first term in the exponential is related to the void growth and the second one to the shearing of the voids. Equation 3 has been applied to cases where the holes are at 45° to the tensile axis using the void dimensions shown in Figure 1(c). The results, shown in Table 4 are in good agreement with the experimental values. It should also be noticed that there is more discrepancy in between the model and the experimental results when only two holes are considered. This is due to constraining effects which prevent the holes from shearing freely at 45° as already discussed in section 3.1.

Table 4: Experimental coalescence strains (defined as $ln(a/a_0)$) for hole configurations at 45° and the corresponding predictions from the McClintock model.

Configuration	Experiment	McClintock	
	Strain	Strain	% diff.
2holes-45°-2W=26 μm	1.36±0.025	1.18	-13%
Array-45°-2W=34 μm	1.33±0.026	1.25	-6%

6 Discussion and conclusion

The void growth and coalescence analysis carried out in the first part of this paper shows that is it possible to follow in detail the ductile fracture process by in-situ tensile tests on laser drilled materials. Because laser holes can be drilled in virtually all materials and in any location, comparisons between the coalescence mechanisms of different materials and void configurations can be made.

Optical microscopy observations using Nomarski contrast allowed the visualization of the slip pat-

Table 3: Experimental coalescence strains (defined as $ln(a/a_0)$) for various hole configurations and the corresponding predictions from the Brown and Embury model and the Thomason model.

Configuration	Experiment	Brown and Embury		Thomason	
	Strain	Strain	% diff.	Strain	% diff.
2holes-90°-2W=37 μm	1.18±0.030	1.20	+2%	0.65	-45%
2holes-45°-2W=26 μm	1.36±0.025	0.83	-39%	0.55	-59%
Array-90°-2W=48 μm	1.39±0.024	1.47	+6%	0.91	-34%
Array-45°-2W=34 μm	1.33±0.026	1.12	-16%	0.67	-49%
1line-90°-2W=40 μm	1.25±0.028	1.25	0%	0.66	-47%
3line-90°-2W=40 μm	1.26±0.033	1.28	+2%	0.77	-39%
7line-90°-2W=40 μm	1.27±0.033	1.28	+1%	0.79	-38%
13line-90°-2W=40 μm	1.29±0.033	1.27	-2%	0.8	-38%
2holes-90°-2W=15 μm	0.51±0.056	0.39	-23.5%	0.17	-66%
2holes-90°-2W=25 μm	0.99±0.040	0.83	-16%	0.51	-48%
2holes-90°-2W=40 μm	1.25±0.211	1.28	+2%	0.66	-47%
2holes-90°-2W=50 μm	1.43±0.026	1.47	+3%	0.90	-37%

tern between the voids and showed a strong localization of the deformation in micro shearbands between voids at 45°. Such a technique could be employed in-situ under the optical microscope in further study, to obtain information on the extent and location of plastic deformation as a function of deformation and hole orientation. This might be especially useful when investigating the slip behavior of material having strong crystal plasticity effects.

It has been shown that the hole spacing and orientation, the nucleation of secondary voids, the yield stress and the work hardening rate have an important effect on coalescence. We quantified the decrease in coalescence strains with decreasing hole spacing and observed two types of coalescence depending on the holes orientation (internal necking versus shear localization). It is however still not clear if the lower failure strains of the Glidcop samples are due to the higher yield stress of Glidcop which results an earlier localization strain or if they are due to the void nucleating particles. Comparing materials of similar yield stress and having one with void nucleating particles and one without might shine some light on the coalescence mechanisms in materials containing a second population of void nucleating particles.

We also demonstrated that constraining effects (due to the number of holes) have a negligible impact on the local coalescence strains for holes oriented at 90° to the tensile axis. However constraining effects are important when the holes are at 45° in that they prevent coalescence by complete shearing of the voids. It would be a challenge to take this effect into account in modelling efforts as it would require the knowledge of the whole sample microstructure (to know how many voids are in the shearing direction) and a criteria for the transition between the shear and normal type of ductile fracture in the ligament between voids.

Even though the experimental results provide a lot of information on void growth and coalescence, it is still difficult to observe coalescence experimentally. The reason is that the parameters extracted from the hole geometry vary smoothly with deformation. In this study, we therefore decided to define coalescence as the intervoid ligament failure strain which is a reproducible and tractable event. However, models in the literature define coalescence as a localization of plastic deformation in the ligament between neighboring voids, which occurs at more or less lower strains than the ligament failure. This could partly explain the differences observed between the Thomason model for void coalescence and the ex-

perimental ligament failure strain values. A post-localization regime such as that proposed by Pardoen and Hutchinson [20] would be required to predict the ligament failure strains but this is out of the scope of the present contribution.

The excellent results provided by the Brown and Embury model could be an outcome of the slip line field approach. Indeed, coalescence (in terms of the plastic limit load of Thomason [32]) can begin before slip lines at 45° are formed but once the 45° slip line condition is met, the constraint in the ligament between the holes is lost and coalescence can terminate rapidly. This could explain why the Brown and Embury results provide values closer to the experimental failure strains and why the Thomason model underestimates them. The McClintock criterion for coalescence by shear is based on a similar assumption as the Brown and Embury model in that coalescence starts when the size of the voids and the ligament between voids become nearly equal, hence the reasonable predictions.

Free surface effects could also influence the present results. Three-dimensional experiments have been carried out [36] that allow to have the holes in the bulk of the sample and therefore eliminate free surface effects. These experiments are closer to the geometry found in real materials but are more difficult to implement. The two-dimensional approaches presented in this paper are therefore necessary in terms of the amount of information that can be obtained and because they can provide additional information such as the slip behavior between the voids as shown in Figure 4.

Finally, crystal plasticity related effects have been neglected in this paper because we observed that all voids behaved in a similar manner. However, the method presented here could be used to investigate the importance of crystal anisotropy on hole growth and coalescence in materials more prone plasticity related effect such as titanium and magnesium.

Acknowledgement

We gratefully acknowledge the support of the Natural Sciences and Engineering Research Council of Canada (NSERC).

References

[1] Goods S., Brown L. Acta Metallurgica 1979; 27: 1-15.

[2] Babout L., Ludwig W., Maire E., Buffière J. Nuclear Instruments and Methods in Physics Research Section B 2003; 200: 303-307.

[3] Argon A.S., Im J., Safoglu R. Metallurgical Transactions A 1975; 6A: 825-837.

[4] Puttick K.E. Philosophical Magazine 1959; 4: 964-969.

[5] Floreen S., Hayden H. Scripta Metallurgica 1970; 4: 87-94.

[6] Cox T.B., Low J.R.J. Metallurgical Transactions 1974; 5: 1457-1470.

[7] McClintock F. J. Appl. Mech. 1968; 35: 363-371.

[8] Rice J., Tracey D. Journal of the Mechanics and Physics of Solids 1969; 201-217.

[9] Worswick M.J., Pick R.J. Journal of the Mechanics and Physics of Solids 1990; 38: 601-625.

[10] Huang Y. Journal of Applied Mechanics 1991; 58: 1084-85.

[11] Gurson A. Journal of Engineering Materials and Technology 1977; 99: 2-15.

[12] Thompson A. Metallurgical Transactions A 1987; 18A: 1877-1886.

[13] Knott J. Metal Science 1980; 327–336.

[14] Park I.-G., Thompson A.W. Acta Metallurgica 1988; 36: 1653-1664.

[15] Marini B., Mudry F., Pineau A. Engineering Fracture Mechanics 1985; 22: 989-996.

[16] Brown M., Embury D. In: Proceedings of 3rd International Conference on Strength of Metals and Alloys 1973; Institute of Metals, London: 164-169.

[17] Needleman A., Tvergaard V. Journal of the Mechanics and Physics of Solids 1984; 32: 461-490.

[18] Thomason P. Journal of the Institute of Metals 1968; 96: 360-365.

[19] Zhang, Z.L. and Niemi, E. (1994) A new failure criterion for the Gurson-Tvergaard dilational constitutive model, International Journal of Fracture, 70:321-334

[20] Pardoen, T. and Hutchinson, J.W. (2000) An extended model for void growth and coalescence, Journal of the Mechanics and Physics of Solids, 48:24672512

[21] Gologanu, M. and Leblond, J.-B. and Perrin, G. and Devaux, J. (2001) Theoretical models for void coalescence in porous ductile solids. I. Coalescence "in layers", International Journal of Solids and Structures, 38:5581-5594

[22] Gologanu, M. and Leblond, J.-B. and Devaux, J. (2001) Theoretical models for void coalescence in porous ductile solids. II. Coalescence "in columns", International Journal of Solids and Structures, 38:5595-5604

[23] Benzerga, A.A. (2002) Micromechanics of coalescence in ductile fracture, Journal of the Mechanics and Physics of Solids, 50:1331-1362,

[24] Pineau, A. (2006) Development of the Local Approach to Fracture over the Past 25 years: Theory and Applications, International Journal of Fracture, 138:139-166

[25] Pineau, A. and Pardoen T. in Comprehensive Structural Integrity, 2nd ed., Elsevier, New York, NY, (2007), 2:684797

[26] Babout L., Maire E., Buffière J., Fougères R. Acta Materialia 2001; 49: 2055-2063.

[27] Gammage J., Wilkinson D., Brechet Y., Embury D. Acta Materialia 2004; 52: 52555263.

[28] Magnusen P.E., Dubensky E.M., Koss D.A. Acta Metallurgica 1988; 36: 1503-1509.

[29] Jia S., Povirk G. International Journal of Solids and Structures 2002; 39: 25332545.

[30] Nagaki S., Nakayama Y., Abe T. International Journal of Mechanical Sciences 1998; 40: 215-226.

[31] Weck A., Crawford T.H.R., Borowiec A., Wilkinson D.S., Preston J.S. Applied Physics A-Materials Science and Processing 2007; 86: 55-61.

[32] Thomason P.F. Ductile Fracture of Metals. Oxford: Pergamon Press; 1990.

[33] Mulholland M., Ege E., Khraishi T., Horstemeyer M., Shen Y.-L. Materials Science and Engineering A 2003; 360: 160-168.

[34] Hill R. Journal of the Mechanics and Physics of Solids 1952; 1: 19-30.

[35] McClintock F.A., Kaplan S.M., Berg C.A. International Journal of Fracture Mechanics 1966; 2: 614-627.

[36] Weck A., Wilkinson D.S., Maire E., Toda H. Submitted for publication in Acta Materialia 2007.